



Size-resolved cloud condensation nuclei (CCN) activity and closure analysis at the HKUST Supersite in Hong Kong

J. W. Meng¹, M. C. Yeung², Y. J. Li^{1,*}, B. Y. L. Lee¹, and C. K. Chan^{1,2}

¹Division of Environment, The Hong Kong University of Science and Technology, Clear Water Bay, Hong Kong SAR, China

²Department of Chemical and Biomolecular Engineering, The Hong Kong University of Science and Technology, Clear Water Bay, Hong Kong SAR, China

* current address: School of Engineering and Applied Sciences, Harvard University, Cambridge, USA

Correspondence to: C. K. Chan (keckchan@ust.hk)

Received: 6 March 2014 – Published in Atmos. Chem. Phys. Discuss.: 3 April 2014

Revised: 20 August 2014 – Accepted: 25 August 2014 – Published: 26 September 2014

Abstract. The cloud condensation nuclei (CCN) properties of atmospheric aerosols were measured on 1–30 May 2011 at the HKUST (Hong Kong University of Science and Technology) Supersite, a coastal site in Hong Kong. Size-resolved CCN activation curves, the ratio of number concentration of CCN (N_{CCN}) to aerosol concentration (N_{CN}) as a function of particle size, were obtained at supersaturation (SS) = 0.15, 0.35, 0.50, and 0.70 % using a DMT (Droplet Measurement Technologies) CCN counter (CCNc) and a TSI scanning mobility particle sizer (SMPS). The mean bulk size-integrated N_{CCN} ranged from $\sim 500 \text{ cm}^{-3}$ at SS = 0.15 % to $\sim 2100 \text{ cm}^{-3}$ at SS = 0.70 %, and the mean bulk N_{CCN} / N_{CN} ratio ranged from 0.16 at SS = 0.15 % to 0.65 at SS = 0.70 %. The average critical mobility diameters (D_{50}) at SS = 0.15, 0.35, 0.50, and 0.70 % were 116, 67, 56, and 46 nm, respectively. The corresponding average hygroscopic parameters (κ_{CCN}) were 0.39, 0.36, 0.31, and 0.28. The decrease in κ_{CCN} can be attributed to the increase in organic to inorganic volume ratio as particle size decreases, as measured by an Aerodyne high resolution time-of-flight aerosol mass spectrometer (HR-ToF-AMS). The κ_{CCN} correlates reasonably well with κ_{AMS_SR} based on size-resolved AMS measurements: $\kappa_{AMS_SR} = \kappa_{org} \times f_{org} + \kappa_{inorg} \times f_{inorg}$, where f_{org} and f_{inorg} are the organic and inorganic volume fractions, respectively, $\kappa_{org} = 0.1$ and $\kappa_{inorg} = 0.6$, with a R^2 of 0.51.

In closure analysis, N_{CCN} was estimated by integrating the measured size-resolved N_{CN} for particles larger than D_{50} derived from κ assuming internal mixing state. Estimates using κ_{AMS_SR} show that the measured and predicted N_{CCN} were

generally within 10 % of each other at all four SS. The deviation increased to 26 % when κ_{AMS} was calculated from bulk PM_{10} AMS measurements of particles because PM_{10} was dominated by particles of 200 to 500 nm in diameter, which had a larger inorganic fraction than those of D_{50} (particle diameter < 200 nm). A constant $\kappa = 0.33$ (the average value of κ_{AMS_SR} over the course of campaign) was found to give an N_{CCN} prediction within 12 % of the actual measured values. We also compared N_{CCN} estimates based on the measured average D_{50} and the average size-resolved CCN activation ratio to examine the relative importance of hygroscopicity and mixing state. N_{CCN} appears to be relatively more sensitive to the mixing state and hygroscopicity at a high SS = 0.70 % and a low SS = 0.15 %, respectively.

1 Introduction

Atmospheric aerosols can act as cloud condensation nuclei (CCN) and affect cloud formation by influencing the CCN number concentration (N_{CCN}) and the size of cloud droplets. Whether aerosol particles will eventually form cloud droplets under a set atmospheric condition mainly depends on their size, chemical composition, and mixing states. Predicting N_{CCN} usually involves measuring the aerosol size distribution and making assumptions about the chemical composition associated to mixing state. Bulk chemical compositions and an assumption of internal mixing state (i.e., particles are identical mixtures of all participating species) are often used in predicting N_{CCN} (Moore et al., 2012a; Wang et al., 2010).

Ambient aerosols are complex mixtures and the aerosol compositions vary substantially with particle size. The hygroscopicity parameter (κ) is used to represent the effect of chemical composition on CCN activity (Petters and Kreidenweis, 2007, 2013). Size-resolved chemical compositions give a size-dependent κ which leads to better N_{CCN} predictions than those based on bulk compositions (Medina et al., 2007; Stroud et al., 2007; Wang et al., 2010).

While the real-time aerosol size-resolved chemical compositions such as non-refractory (NR)-species and black carbon (BC) can be obtained with an aerosol mass spectrometer and a single particle soot photometer, respectively, information on the mixing state is usually not available or incomplete. Various assumptions have been applied to describe the aerosol mixing state (Asa-Awuku et al., 2011; Bougiatioti et al., 2009; Cubison et al., 2008; Ervens et al., 2010; Lance et al., 2009; Latham et al., 2013; Moore et al., 2012a; Rose et al., 2011; Wang et al., 2010). N_{CCN} predictions assuming internal mixing are usually larger than measured values by 20 % or even more, since this assumption overestimates the contribution of organics to N_{CCN} (Rose et al., 2011; Wang et al., 2010; Wex et al., 2010). Another extreme assumption is external mixing, which is when the aerosol contains different types of particles but each particle consists of a single species (Textor et al., 2006; Zhang et al., 2010). Under this assumption, the number concentration (N_{CN}) of each type of particles is determined as the product of the total N_{CN} and the volume fraction of the species. The D_{50} of a species is calculated based on its κ (Moore et al., 2012a; Wang et al., 2010) and N_{CCN} is obtained by integrating N_{CN} above D_{50} . Finally, the total N_{CCN} is calculated by adding up all the predicted N_{CCN} of the species. This simplified external mixing state assumption could underestimate N_{CCN} . For example, Wang et al. (2010) reported an underestimation of $\sim 20\%$ in N_{CCN} at supersaturation (SS) from 0.11 to 0.35 %. Aerosol mixing state and chemical composition are thus important factors that need to be considered in the CCN prediction, especially in places where anthropogenic aerosol emission is strong and pollution is heavy (Ervens et al., 2010; Kammermann et al., 2010; Kerminen et al., 2012; Rose et al., 2010; Wang et al., 2010).

Measurements of the condensation nuclei (CN) and CCN spectra simultaneously by combining a scanning mobility particle sizer (SMPS) and a CCN counter (CCNc) have been made (Asa-Awuku et al., 2010; Lance et al., 2009; Moore et al., 2010, 2012a; Padró et al., 2010; Rose et al., 2010). The size-resolved CCN activation ratios, i.e., the fraction of the measured $N_{\text{CCN}}/N_{\text{CN}}$ as a function of particle size, are the combined results of the size distribution, size resolved chemical composition, and the mixing state of the aerosols. Recently, Deng et al. (2013) estimated N_{CCN} by integrating the product of the measured size-distributed N_{CN} and the averaged size-resolved CCN activation ratio at each particle size bin measured at Wuqing in the North China Plain. The

estimated and measured values differed by less than 6 % at SS = 0.06 to 0.81 %.

The rapid urbanization and industrial development in the Pearl River delta (PRD) have resulted in heavy air pollution, especially particulate matter (PM) pollution (Chan and Yao, 2008). Hong Kong, a typical coastal city southeast of the PRD, is affected by PM due to both local anthropogenic emissions and transportation of pollutants from the PRD (Li et al., 2014).

In this study, we report for the first time size-resolved measurements of CCN activity in Hong Kong. We correlated the CCN-derived hygroscopicity (κ_{CCN}) with those estimated from the size-dependent aerosol chemical compositions determined by an Aerodyne high-resolution time-of-flight aerosol mass spectrometer (HR-ToF-AMS, hereafter as AMS). Assuming internal mixtures, we carried out closure studies on N_{CCN} prediction based on the size-distributions of N_{CN} measured by a TSI SMPS and on the hygroscopicity values derived from size resolved and size integrated chemical compositions measured by AMS using Köhler theory, κ_{AMS} , and some assumed constants. Finally, using the average D_{50} and the size-resolved CCN activation ratios from the CCN measurements, we examined the relative importance of hygroscopicity and mixing state in N_{CCN} predictions at different SS. Hygroscopicity is technically a property of aerosols and it is determined by their chemical composition, mixing state, and size distribution. In this paper, we refer hygroscopicity as a property of the components, assuming internal mixing, in aerosols for the discussions below.

2 Experimental methods

2.1 Sampling site and meteorological conditions

Measurements of aerosol chemical properties and CCN activity were carried out throughout the entire month of May 2011 at the Air Quality Research Supersite situated on the campus of the Hong Kong University of Science and Technology (HKUST) on the east coast of Hong Kong (see <http://www.envr.ust.hk/research/research-facility/background-materials.html>). High relative humidity (RH) with a mean of 81 % and an average temperature of 26.0 °C prevailed in this study. More information on the sampling location and meteorological conditions is available from Lee et al. (2013) and Li et al. (2013). Hygroscopic tandem differential mobility analyzer (HTDMA) measurements have also been reported at this site (Lopez-Yglesias et al., 2014; Yeung et al., 2014).

2.2 Instrument setup

2.2.1 Sample Inlet System

Ambient air was sampled at a flow rate of 16.67 L min⁻¹ after passing through a PM_{2.5} cyclone on the roof of the

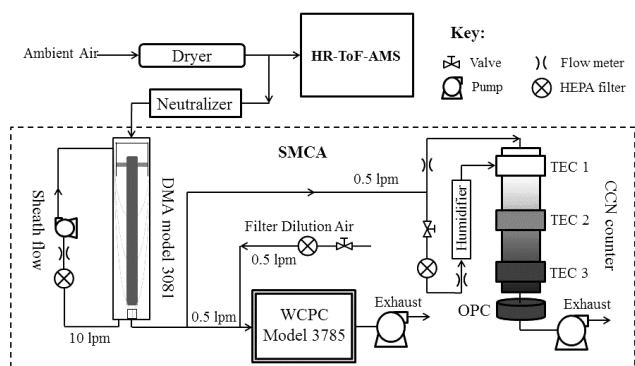


Figure 1. Schematic of the experimental setup for size-resolved CCN activation and chemical composition measurement.

supersite (appropriately 20 m above sea level) and into a stainless steel sampling port supplying the online instruments of the TSI SMPS, the Droplet Measurement Technologies (DMT) dual column continuous-flow CCN counter (CCNc-200) and the Aerodyne AMS. The sampled air passed through a 1 m long diffusion drier (Brechtel Manufacturing Inc., San Francisco, CA) filled with silica gel, thus its RH was below 30% before it went into the above instruments for measurements.

2.2.2 CCN measurements

Size-resolved CCN spectra and activation ratios were measured with the CCNc-200 (Lance et al., 2006; Roberts and Nenes, 2005) coupled with a TSI SMPS, consisting of a differential mobility analyzer (DMA, TSI 3081L) and a water-based condensation particle counter (WCPC, TSI 3785).

As shown in Fig. 1, charge-neutralized aerosols passed through the DMA for classification. The classified aerosols were then split into two streams: with one going into the WCPC for N_{CN} measurements and the other into the CCNc-200 for N_{CCN} measurements. The particle size distribution was measured every 6 min, with an up-scan time of 300 s. The sample flow rate was 1 L min^{-1} for the DMA, 0.5 L min^{-1} for the WCPC and the CCNc-200 each, and the closed-loop sheath air flow rate was 10 L min^{-1} . These flow rate settings allow SMPS (DMA + WCPC) measurements for particles ranging from 7 to 300 nm in mobility diameter (D_m), which as we will show later, cover the D_{50} (D_m) range of the particles studied. The sheath flow rate was continuously corrected using a mass flow controller. All flow rates were regularly checked and sizing accuracy for the SMPS and the CCNc-200 was verified with polystyrene latex (PSL) spheres.

The CCNc-200 was operated at a total flow rate of 1 L min^{-1} , of which 0.5 L min^{-1} was for column A connected to the DMA to measure the size-resolved CCN spectrum and another 0.5 L min^{-1} was for column B connected to the sample inlet system to measure the total N_{CCN} . A sheath-

to-aerosol flow ratio of 10 was used. Lathem and Nenes (2011) pointed out that the direct measurements could lead to underestimations of bulk N_{CCN} due to the depletion of water inside the column by a large amount of aerosols. In our measurements, the bulk N_{CCN} integrated from size-resolved CCN measurement using column A are usually fewer than 5000 cm^{-3} and they correlate well with that from the direct measurement using column B with a slope of 0.97 and correlation coefficient (R^2) of 0.53 as shown in Fig. S1 in the Supplement. We use bulk N_{CCN} calculated from column A for the comparison with N_{CN} from SMPS and for the closure study below. For every measurement cycle, four SS (0.15, 0.35, 0.50, and 0.70%) were selected. Measurements at SS = 0.15 lasted 22 min whereas those at other SS lasted 12 min each for repeatability. CCNc temperature transients during SS changes are known to produce unreliable spectra if they occur during a voltage up-scan (Moore et al., 2010). In our measurements, the instrument profiles were allowed up to ~ 2 min to stabilize whenever the temperature gradient was changed. At SS = 0.15%, a longer time (~ 4 min) was required for the stabilization of temperatures. Only data collected under stabilized temperatures were used for analysis.

The CCNc-200 was calibrated with size selected DMA ammonium sulfate particles at the four SS (Deng et al., 2011; Rose et al., 2008) regularly during the campaign. The instrument SS was derived from Köhler theory using a constant van't Hoff factor of 2.5 for ammonium sulfate (Low, 1969; Tang and Munkelwitz, 1994; Young and Warren, 1992).

2.2.3 Aerosol chemical compositions

Non-refractory PM_{10} (NR- PM_{10}) constituents of sulfate, nitrate, ammonium, chloride, and organics were measured with the AMS operated under V, particle time of flight (pToF), and W modes. The principle behind the instrument has been described in detail elsewhere (DeCarlo et al., 2006) and will only be briefly described here. In pToF mode, the instrument performs particle sizing based on particle time-of-flight with the aid of a chopper and gives size-resolved chemical composition data in vacuum aerodynamic diameter (D_{va}) (DeCarlo et al., 2004). In V mode, the shorter traveling path for ions in the ion time-of-flight (ToF) chamber gives a mass spectral resolving power of approximately 2000 (DeCarlo et al., 2006) and better sensitivity. In W mode, the mass spectral resolving power is approximately 4000 (DeCarlo et al., 2006) but the signal-to-noise ratio is lower. The instrument was operated alternately between the V + pToF combined mode and the W mode for 5 min each. Evaluation of the ionization efficiency (IE) was carried out with ammonium nitrate particles weekly and both the flow rate and particle sizing were calibrated before and after the campaign. A more detailed description of the performance of the AMS during the campaign is presented by Li et al. (2013) and Lee et al. (2013). The AMS only measures NR-species but not elemental carbon (EC), sea salt, or crustal species. However, EC only accounts for

less than 5 % of the PM₁ mass and hence can be neglected (Huang et al., 2014; Lee et al., 2013). Sea salt and crustal species typically exist in the coarse mode and make negligible contributions to PM₁.

2.3 Data analysis

2.3.1 CN and CCN data

The time series of N_{CN} and N_{CCN} distributions were obtained using the TSI Aerosol Instrument Manager (AIM) software (Wang and Flagan, 1990) and CCN acquisition software, respectively. The data collected during the voltage up-scan were employed for the inversion. The scanning mobility CCN analysis (SMCA) was employed for calculating the size-resolved CCN activation fractions (Moore et al., 2010). The ratio of N_{CCN} to N_{CN} gives the size-resolved CCN activation fraction at each size. Then, the size-resolved CCN activation ratio was obtained by fitting the activation fraction with the sigmoidal function described by Eq. (1) (see Sect. 3.3) (Moore et al., 2010; Padró et al., 2010).

2.3.2 HR-ToF-AMS data

The standard toolkit of SQUIRREL (Sueper, 2011) was used for AMS data analysis. The collection efficiency (CE) used for this work was 0.5 and the relative ionization efficiency (RIE) of 1.2 for sulfate, 1.1 for nitrate, 1.3 for chloride, 1.4 for organics and 4.0 for ammonium were used as described by Li et al. (2013) and Lee et al. (2013). The size-resolved mass spectra for vacuum aerodynamic diameter (D_{va}) ranging from 50 to 2000 nm (DeCarlo et al., 2004) were obtained every 5 min on average. The mass concentration of each size bin was obtained by averaging with the two adjacent size bins to reduce the influence of noise (Rose et al., 2011). In order to relate the size-resolved AMS data to those of SMPS and CCNc measurements directly, the AMS D_{va} size was divided by a factor of 1.7 to obtain the corresponding mobility equivalent diameter (D_{m}) (Cheng et al., 2006; DeCarlo et al., 2004). The volume fractions of size-resolved and bulk chemical compositions were calculated from the mass concentrations using densities of organics and inorganics of 1.3 g cm⁻³ and 1.75 g cm⁻³, respectively (Alfarra et al., 2006; Cross et al., 2007; Gunthe et al., 2009; King et al., 2007).

2.3.3 D_{50} , κ_{CCN} and κ_{AMS}

The critical diameter D_{50} , also known as the activation diameter, is the diameter at which 50 % of the particles are activated at a specific SS. The D_{50} of a simple sigmoidal shaped activation ratio curve is determined by fitting the size-resolved activation fractions with the equation below:

$$\frac{N_{\text{CCN}}}{N_{\text{CN}}} = \frac{B}{1 + \left(\frac{D_{\text{p}}}{D_{50}}\right)^c}, \quad (1)$$

where D_{p} is the dry mobility diameter, B , c , and D_{50} are fitting coefficients that describe the asymptote/plateau, the slope, and the inflection point of the sigmoid, respectively (Moore et al., 2010; Padró et al., 2012). The values of B were more than 90 % during the whole campaign, indicating most of the particles were in the internal mixing state (Mei et al., 2013).

The measured hygroscopic parameter (κ_{CCN}) is determined from D_{50} by the following equation:

$$\kappa_{\text{CCN}} = \frac{4A^3\sigma^3s/a(T)}{27T^3D_{50}^3\ln^2S_c}, \quad (2)$$

where $A = 8.69251 \times 10^{-6} \text{ K m}^3 \text{ J}^{-1}$, is the temperature-dependent surface tension of the solution/air interface, T is temperature, and S_c is the critical saturation ratio. Pure water surface tension is assumed in the calculations of κ_{CCN} in this paper (Petters and Kreidenweis, 2013; Sullivan et al., 2009).

The hygroscopic parameter κ_{AMS} can be obtained from AMS measurements using

$$\kappa_{\text{AMS}} = \kappa_{\text{org}} \times f_{\text{org}} + \kappa_{\text{inorg}} \times f_{\text{inorg}}, \quad (3)$$

where f_{org} and f_{inorg} are the organics and inorganics volume fraction derived from AMS measurements (Petters and Kreidenweis, 2007). Bulk κ_{AMS} (hereafter $\kappa_{\text{AMS,B}}$) and size-resolved κ_{AMS} (hereafter $\kappa_{\text{AMS,SR}}$) are obtained from the corresponding bulk and size-resolved volume fractions of organics and inorganics, respectively. Also, it was assumed that $\kappa_{\text{inorg}} = 0.6$ for the whole campaign, $\kappa_{\text{org}} = 0.2$ for the hazy period and $\kappa_{\text{org}} = 0.1$ for the foggy and non-episode periods.

The time-series hygroscopicities derived from bulk and size-resolved AMS measurements are shown in Fig. S2 in the Supplement. $\kappa_{\text{AMS,B}}$ were larger than $\kappa_{\text{AMS,SR}}$ in all four SS because bulk AMS compositions biased towards the inorganics as discussed below. Their difference increases as SS increases because the corresponding D_{50} decreases and these smaller particles have a larger fraction than the bulk has.

3 Results and discussion

3.1 Overview

Figure 2 shows an overview of the bulk N_{CCN} concentrations and $N_{\text{CCN}}/N_{\text{CN}}$ activation ratio at SS of (a) 0.15 %, (b) 0.35 %, (c) 0.50 %, and (d) 0.70 %, as well as (e) the bulk N_{CN} and the NR-PM₁ total and component mass concentration and (f) the volume fractions of the AMS chemical components over the entire month of May 2011. Statistics of the measurements are given in Table 1. The gaps in the data in Fig. 2 are due to instrument downtime. For most of the time, the total N_{CCN} at SS of 0.15, 0.35, 0.50 and 0.70 % were below 800, 3000, 5000 and 5600 cm⁻³ respectively, and N_{CN} was below 10 000 cm⁻³. Both N_{CCN} and N_{CN} in this study are lower than those observed in July 2006 in Guangzhou, a

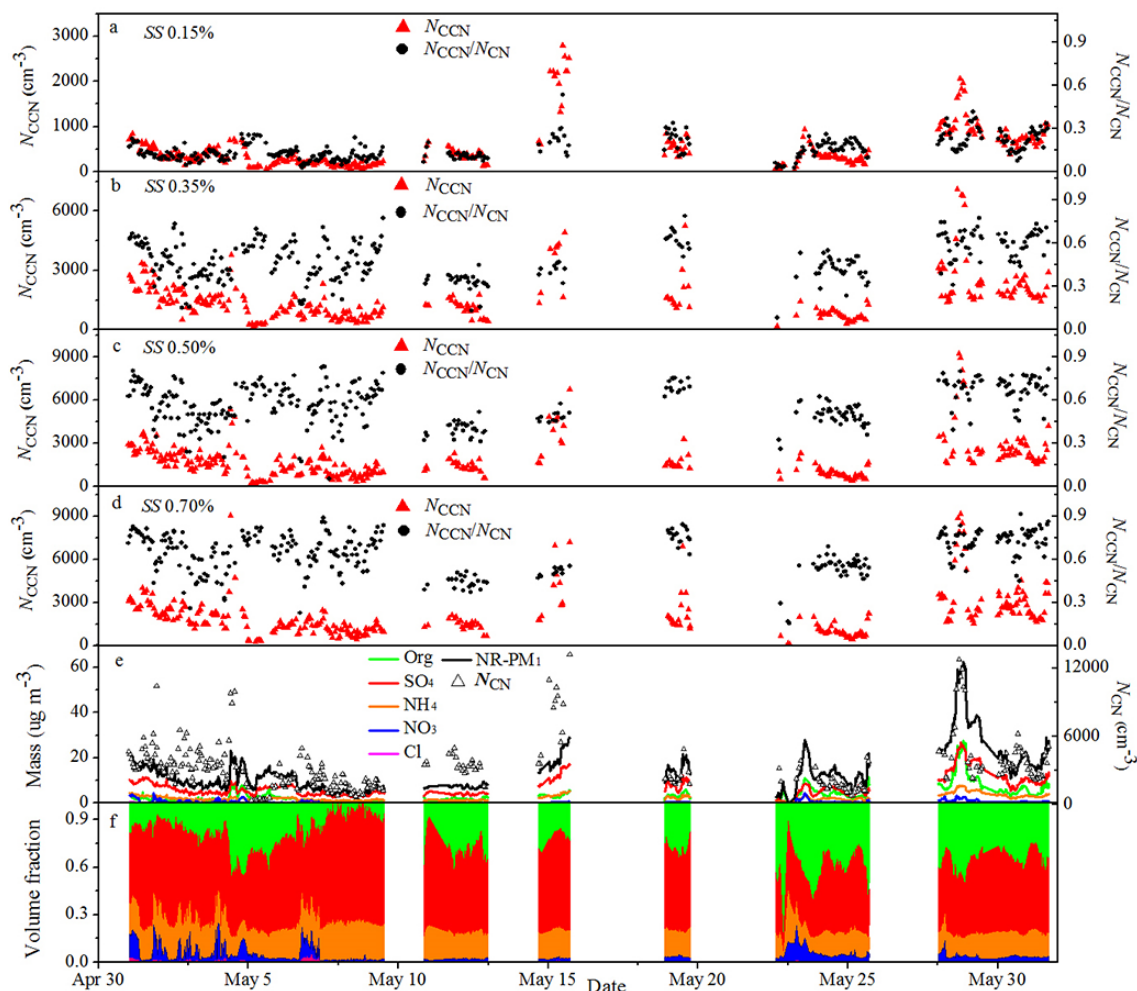


Figure 2. The N_{CCN} and the N_{CCN} / N_{CN} ratio at SS of (a) 0.15 %, (b) 0.35 %, (c) 0.50 %, and (d) 0.70 %; (e) N_{CN} and NR-species mass concentrations from CCNc, SMPS and AMS; (f) NR-species volume fractions derived from AMS.

nearby city in southern China (Rose et al., 2010). The bulk N_{CCN} / N_{CN} ratio was as low as 0.03 at $SS = 0.15\%$, but it was as high as 0.92 at $SS = 0.70\%$. Even at the same SS, the bulk N_{CCN} , N_{CN} and N_{CCN} / N_{CN} ratio varied greatly during the campaign.

The bulk mass concentrations of NR-PM₁ ranged from $0.8 \mu\text{g m}^{-3}$ to $62.4 \mu\text{g m}^{-3}$ with a mean value of $14.5 \pm 9.7 \mu\text{g m}^{-3}$ as shown in Fig. 2e. The average bulk volume fractions of NR-species were $53 \pm 10\%$, $25 \pm 13\%$, $18 \pm 4\%$, $4 \pm 3\%$ for sulfate, organics, ammonia, and nitrate, respectively (Lee et al., 2013). The bulk mass concentrations for all NR-species were in general low during the campaign compared with those reported for the PRD region (Gong et al., 2012; Rose et al., 2011; Takegawa et al., 2009; Xiao et al., 2011).

There were two periods of particular interest during this campaign: one was a foggy period (15 May) and the other was a hazy period (28–30 May). The division of the month of May in 2011 into foggy, hazy and non-episode periods was

based on differences in meteorology, such as RH, temperature and cloud cover, and mass concentration and the O : C ratio. On average, the foggy period had a high RH (91.1 %), a low temperature (23.3°C) and a high percentage cloud coverage (89.7 %) and a high liquid water content (LWC) in fine particles ($47.5 \mu\text{g m}^{-3}$) as shown in Li et al. (2013). The hazy period had a much lower RH (66.6 %), a higher temperature (26.2°C) and a much lower percentage cloud coverage (43.3 %) and LWC ($17.5 \mu\text{g m}^{-3}$). The slowing surface winds and the establishment of a well-defined land-sea breeze with a gradual daily reversal of wind direction contributed to the accumulation of local and regional pollutants coming from the PRD due to the persistent northerly and northwesterly air masses (Lee et al., 2013).

During the foggy period, the bulk NR-PM₁ was as high as $30 \mu\text{g m}^{-3}$ (Fig. 2e; Li et al., 2013). The hazy period was much less humid and it saw the highest mass concentration of NR-PM₁ species recorded during the whole campaign. It also had the highest degree of oxygenation with an average

Table 1. Statistics of the bulk N_{CCN} (cm^{-3}) at four SS (%) showing the minimum, maximum, mean number concentration, the $N_{\text{CCN}}/N_{\text{CN}}$ ratio, and standard deviation (SD). The last column shows the number of data sets (n) in this campaign.

SS (%)	Max		Min		Mean \pm SD		n
	N_{CCN} (cm^{-3})	$N_{\text{CCN}}/N_{\text{CN}}$	N_{CCN} (cm^{-3})	$N_{\text{CCN}}/N_{\text{CN}}$	N_{CCN} (cm^{-3})	$N_{\text{CCN}}/N_{\text{CN}}$	
0.15	2815	0.54	33	0.03	512 ± 452	0.16 ± 0.08	319
0.35	8055	0.78	186	0.08	1546 ± 1137	0.48 ± 0.14	316
0.50	9156	0.82	210	0.12	1815 ± 1285	0.57 ± 0.14	326
0.70	9268	0.92	280	0.16	2082 ± 1484	0.65 ± 0.14	320

Table 2. The average size-resolved mass concentrations ($\mu\text{g m}^{-3}$, Conc.) and volume fractions (f) of chemical compositions from size-resolved AMS measurements during the foggy, hazy and the non-episode periods. Conc. and f were obtained by integrating over the size range (D_{m}) from 42 to 1200 nm for Fig. 3 a–c and from 42 to 200 nm for Fig. 3 d–f. Data are shown as mean \pm standard deviations.

Period	Organics		Sulfate		Ammonium		Nitrate		Chloride	
	Conc.	f	Conc.	f	Conc.	f	Conc.	f	Conc.	f
Foggy	1.60 ± 1.10	0.39 ± 0.12	4.86 ± 3.51	0.45 ± 0.10	1.33 ± 0.98	0.14 ± 0.04	0.18 ± 0.12	0.03 ± 0.00	0.03 ± 0.02	0.001 ± 0.00
Hazy	4.25 ± 2.52	0.57 ± 0.08	5.96 ± 4.36	0.29 ± 0.06	1.71 ± 1.22	0.08 ± 0.03	0.51 ± 0.27	0.06 ± 0.01	0.02 ± 0.01	0.002 ± 0.00
The rest	1.19 ± 0.71	0.47 ± 0.11	2.65 ± 1.86	0.37 ± 0.08	0.81 ± 0.55	0.12 ± 0.03	0.25 ± 0.15	0.04 ± 0.00	0.02 ± 0.01	0.002 ± 0.00

O : C ratio of 0.51 (Li et al., 2013). During the hazy period, the mean bulk N_{CCN} ranged from 1100 cm^{-3} with bulk $N_{\text{CCN}}/N_{\text{CN}}$ of 0.22 at SS = 0.15 % to 5300 cm^{-3} with bulk $N_{\text{CCN}}/N_{\text{CN}}$ of 0.72 at SS = 0.70 %. During non-episode periods, the mean bulk N_{CCN} ranged from 300 cm^{-3} with bulk $N_{\text{CCN}}/N_{\text{CN}}$ of 0.14 at SS = 0.15 % to 2700 cm^{-3} with bulk $N_{\text{CCN}}/N_{\text{CN}}$ of 0.61 at SS = 0.70 %.

3.2 f , κ_{CCN} and κ_{AMS}

The average size-resolved mass distributions and volume fractions (f) of NR-PM₁ calculated from AMS measurements are shown in Fig. 3a–c and d–f, respectively, for the foggy period, the hazy period, and the non-episode periods. The NR-PM₁ showed a major mode at the dry particle size (D_{m} , hereafter, diameters shown are D_{m}) of $\sim 285 \text{ nm}$ in the foggy period, at $\sim 355 \text{ nm}$ in the hazy period and at $\sim 325 \text{ nm}$ in the non-episode periods. Sulfate and organics accounted for large mass fractions (78 % in total) during the whole campaign as shown in Table 2. Sulfate dominated in the foggy period, contributing to a volume fraction of 0.45 for 42–200 nm particles. Organics and nitrate often had a shoulder at a small size mode at 100 to 130 nm. This shoulder was obvious in the hazy period and non-episode periods but not so in the foggy period. On average, this smaller mode accounted for 11 and 12 % of organics and nitrate, respectively. On the other hand, only 2 % of sulfate was found in this mode (Lee et al., 2013).

Figure 3d–f show the average size-resolved volume fraction distributions of the AMS aerosol compositions from 42 to 200 nm in the foggy period, the hazy period and the non-episode periods. The volume fraction of organics decreased, while the inorganics increased with particle size. Overall, the size-resolved volume fractions of organics ranged from 0.73

at 42 to 0.25 at 200 nm. Additionally, the bulk volume ratio of organics to inorganics between 42 and 200 nm was 0.65 in the foggy period, 1.33 in the hazy period, and 0.87 in the non-episode periods.

The measured κ_{CCN} (yellow symbols) and the calculated $\kappa_{\text{AMS_SR}}$ (blue symbols), in the form of median values and interquartile ranges, are plotted against their corresponding D_{50} in Fig. 3d–f. The median and mean values of κ_{CCN} and $\kappa_{\text{AMS_SR}}$ were essentially the same. Overall, the median D_{50} were 116, 68, 55, and 47 nm, with an interquartile range of less than 16 %, at SS of 0.15, 0.35, 0.50, and 0.70 %, respectively. During the foggy period, which featured high inorganics volume fractions, the median κ_{CCN} were 0.44, 0.37, 0.36 and 0.29 at SS from 0.15 % to 0.70 %. They are higher than the corresponding values in the hazy period (0.38, 0.36, 0.32 and 0.28) and the non-episode periods (0.39, 0.37, 0.33 and 0.27). The difference in κ_{CCN} in these periods was most obvious at SS = 0.15 %, at which D_{50} was around 110 nm, and the corresponding inorganic volume fraction was 0.6 in foggy period, 0.4 in the hazy period and 0.5 in the non-episode period. The high inorganic volume fraction results in high aerosol hygroscopicity.

The $\kappa_{\text{AMS_SR}}$ calculated from Eq. (3) assuming $\kappa_{\text{org}} = 0.1$ and $\kappa_{\text{inorg}} = 0.6$ agreed well with the measured κ_{CCN} in the foggy period and the non-episode periods as shown in Fig. 3d and f. In the hazy period (Fig. 3e), assuming $\kappa_{\text{org}} = 0.2$ and $\kappa_{\text{inorg}} = 0.6$ gave better agreement between $\kappa_{\text{AMS_SR}}$ and κ_{CCN} . The hazy period had a higher O : C ratio of 0.51, compared to 0.43 and 0.39 in foggy and the non-episode periods respectively (Li et al., 2013), leading to a higher hygroscopicity of the organic aerosols (Chang et al., 2010; Lambe et

Table 3. Methods used in N_{CCN} prediction based on the individual CCN scan and average D_{50} over whole period from AMS measurement.

Methods	Mixing state	Chemical composition	κ_{AMS}	D_{50}
I	Internal	Bulk AMS measurements	$\kappa_{\text{AMS}} = 0.1 \times f_{\text{org}} + 0.6 \times f_{\text{inorg}}$	Individual
II	Internal	Bulk AMS measurements	as above	Average
III	Internal	Size-resolved AMS measurements	as above	Individual
IV	Internal	Size-resolved AMS measurements	as above	Average
V	Internal	N/A	0.35/0.33/0.30	Constants

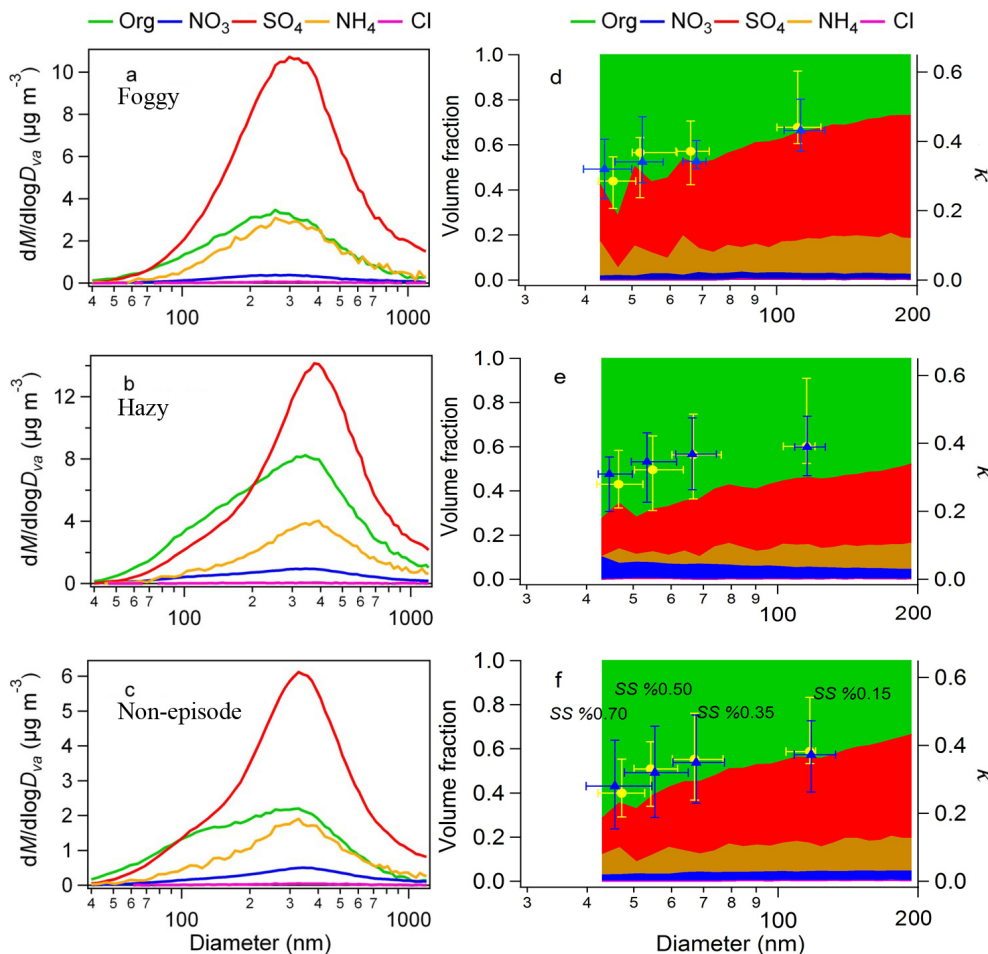


Figure 3. Size-resolved mass concentration distributions of aerosol chemical composition derived from AMS averaged over (a) the foggy period, (b) the hazy period, and (c) the non-episode periods; the corresponding size-resolved volume fractions of aerosol chemical compositions (colored areas), the observed κ_{CCN} (yellow) and the calculated $\kappa_{\text{AMS_SR}}$ (blue) during (d) the foggy period, (e) the hazy period and (g) the non-episode period. Data points median values and interquartile ranges. $\kappa_{\text{inorg}} = 0.6$ in all cases, $\kappa_{\text{org}} = 0.1$ in (d) and (f), $\kappa_{\text{org}} = 0.2$ in (e).

al., 2011; Massoli et al., 2010; Mei et al., 2013; Moore et al., 2012b).

We further examine the correlations between the observed κ_{CCN} and the size-resolved organic volume fraction (f_{org}) in Fig. 4a for the hazy period and Fig. 4b for the rest of the campaign. In order to avoid low signal-to-noise ratios of AMS measurements on the correlation study, only data points with mass concentrations in a size bin of larger than $0.6 \mu\text{g m}^{-3}$

were used. Extrapolation of the least square fit line in Fig. 4a and b to $f_{\text{org}} = 1$ yields $\kappa_{\text{org}} = 0.21 \pm 0.02$ and 0.09 ± 0.01 for the organic fraction and extrapolation to $f_{\text{org}} = 0$ yields $\kappa_{\text{inorg}} = 0.59 \pm 0.03$ and 0.59 ± 0.01 for the inorganic fraction, respectively. These values are close to the characteristic values of organic (0.1) and inorganic hygroscopicity (0.6) in the PRD region (Rose et al., 2011), and to the averaged values of $\kappa_{\text{org}} = 0.1$ and $\kappa_{\text{inorg}} = 0.6\text{--}0.7$ in earlier studies in

Table 4. Overview of N_{CCN} predictions, κ from D_{50} based on CCN measurement and derived from equation 3 based on AMS measurement are shown as mean \pm standard deviation, slope and R^2 are from the least square fit between the calculated N_{CCN} and measured ones.

Categories	Principles	SS (%)	κ	Slope	R^2
CCN _C	The average D_{50} from CCN measurement	0.15	0.39 ± 0.06	1.10	0.94
		0.35	0.36 ± 0.09	1.01	0.95
		0.50	0.31 ± 0.10	1.05	0.97
		0.70	0.28 ± 0.09	1.08	0.98
	The average CCN activation ratio	0.15	–	1.09	0.94
		0.35	–	0.99	0.95
		0.50	–	1.02	0.97
		0.70	–	1.04	0.98
AMS	The D_{50} from $\kappa_{\text{AMS_B}}$	0.15	–	1.21	0.93
		0.35	–	1.06	0.95
		0.50	–	1.13	0.96
		0.70	–	1.17	0.98
	The average D_{50} from $\kappa_{\text{AMS_B}}$	0.15	0.45 ± 0.07	1.26	0.93
		0.35	0.46 ± 0.06	1.08	0.96
		0.50	0.46 ± 0.06	1.13	0.96
		0.70	0.46 ± 0.07	1.18	0.98
	The D_{50} from $\kappa_{\text{AMS_SR}}$	0.15	–	1.06	0.91
		0.35	–	0.94	0.93
		0.50	–	1.03	0.95
		0.70	–	1.10	0.97
	The average D_{50} from $\kappa_{\text{AMS_SR}}$	0.15	0.37 ± 0.07	1.08	0.94
		0.35	0.35 ± 0.08	1.01	0.95
		0.50	0.31 ± 0.07	1.05	0.97
		0.70	0.29 ± 0.09	1.09	0.98
Others	Constant κ	0.15	0.35/0.33/0.30	1.05/0.98/0.91	0.95/0.95/0.95
		0.35	0.35/0.33/0.30	1.01/0.96/0.91	0.95/0.95/0.95
		0.50	0.35/0.33/0.30	1.08/1.05/1.03	0.97/0.97/0.97
		0.70	0.35/0.33/0.30	1.13/1.12/1.11	0.98/0.98/0.98

Beijing and the Gulf of Mexico (Gunthe et al., 2011; Moore et al., 2012b). The average organic hygroscopicity is within the typical range for individual organic species from zero for insoluble organics to 0.3 for soluble organics (Hersey et al., 2011; Lambe et al., 2011; Petters and Kreidenweis, 2007). $\kappa_{\text{AMS_SR}}$ correlates reasonably well with κ_{CCN} , with R^2 of 0.51, as shown in Fig. S3 in the Supplement.

On the other hand, the mean value of $\kappa_{\text{AMS_B}}$ derived from bulk AMS compositions was 0.45 at SS = 0.15 % and 0.46 for the other SS, which are significantly larger than the measured κ_{CCN} ranging from 0.39 to 0.28 for SS of 0.15 % to 0.7 % as shown in Table 4. Size-resolved AMS measurements are needed to accurately determine the hygroscopicity parameter and predict N_{CCN} (Cubison et al., 2008; Moore et al., 2012a). For closure analysis below, we use $\kappa_{\text{org}} = 0.1$ and $\kappa_{\text{inorg}} = 0.6$.

3.3 CCN closure study

The closure studies on N_{CCN} prediction were carried out based on the measured size-resolved N_{CN} distributions and the AMS measurements. In the first approach, we assumed internal mixing and used κ_{AMS} from (i) bulk and (ii) the size-resolved AMS measurements for each data set using Eq. (3), and (iii) assumed constant κ values. The corresponding individual D_{50} was then calculated from these κ estimates using Eq. (2), based on which N_{CCN} was predicted. Furthermore, we also used the average D_{50} over the whole campaign in N_{CCN} prediction. Table 3 summarizes the assumptions and parameters used in these methods. In these cases N_{CCN} was calculated by integrating the measured size-resolved N_{CN} distributions for particles larger than D_{50} . The aim of using the average D_{50} was to test how well it represented the activation properties of aerosol during the campaign. Finally, we examined the relative importance of chemical composition and mixing state in N_{CCN} predictions at different SS by

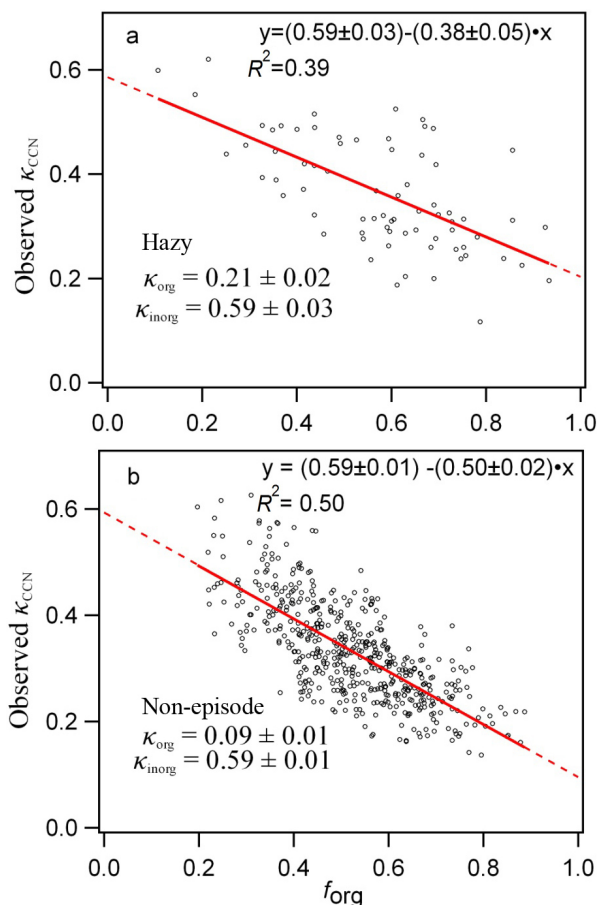


Figure 4. Correlations between the observed κ_{CCN} and the organic volume fraction (f_{org}) determined by size-resolved AMS measurements for the (a) hazy period ($n = 72$) and (b) the non-episode period ($n = 516$). The red line is the linear least squares fit (p value < 0.01).

comparing the N_{CCN} using the average D_{50} with an internal mixing assumption and the size-resolved CCN activation ratios from CCN measurements which reflect the actual mixing state of the aerosols. The last approach involved integrating the product of the measured size-distribution of N_{CN} and the size-resolved CCN activation ratio in each particle size bin.

3.3.1 Prediction of N_{CCN} based on κ_{AMS}

κ_{AMS} from bulk AMS measurements

The hygroscopicity κ_{AMS_B} was estimated by assuming that all particles have the same chemical composition as determined by bulk AMS measurements and $\kappa_{\text{org}} = 0.1$ and $\kappa_{\text{inorg}} = 0.6$. The closure results are shown in Fig. 5(i) a–h and Table 4. Overall, the approaches of using individual D_{50} and the average D_{50} grossly over-predicted N_{CCN} by up to 21 and 26 %, respectively. As shown in Fig. 3a–c, PM_{10} was dominated by inorganic species with the bulk volume frac-

tion as high as 69 % during the whole period. The bulk volume ratio mainly reflects the composition of particles from 200 to 500 nm where inorganic species dominated. On the other hand, D_{50} at the four SS were all less than 200 nm where organic species accounted for more than 39 % of bulk volume fraction as shown in Table 2 and Fig. 3. Therefore, deriving κ_{AMS} from bulk AMS measurements leads to a positive bias toward inorganic species, and hence an overestimation of κ_{AMS_B} and N_{CCN} . Wang et al. (2010) found that the overestimation arising from the use of the bulk mass concentrations decreased from 80 to 39 % when SS decreased from 0.35 to 0.11 %. Our data also shows decreasing overestimation as SS decreases, except for data at $\text{SS} = 0.15$ %, where the N_{CCN} was smaller than 1000 cm^{-3} most of the time. The low counts may have introduced larger uncertainty in the measurements as shown in the Supplement.

κ_{AMS} from size-resolved AMS measurements

Figure 5(ii) a–d and e–h show the correlations between the measured N_{CCN} and the N_{CCN} predicted from the individual D_{50} of each data set and the averaged D_{50} derived from κ_{AMS_SR} , respectively. The slope and R^2 are given in Table 4. In general, the N_{CCN} prediction deviated by 10 % or less for both approaches, a substantial improvement compared to those using κ_{AMS_B} , and the average D_{50} adequately reflects the aerosol activation properties. At $\text{SS} = 0.70$ %, individual D_{50} and the average D_{50} gave the close deviations of 10 and 9 % respectively between the measured and predicted N_{CCN} . At high SS, where even particles of moderate hygroscopicity are activated (Kim et al., 2011), the N_{CCN} prediction is less sensitive to hygroscopicity than at low SS. The difference of the deviations increased as SS decreased from 0.70 to 0.35 %. At lower SS, differences in hygroscopicity as reflected from the different D_{50} used in the calculations gave larger differences in N_{CCN} predictions.

The overestimation from using the average D_{50} decreased from 9 % at SS of 0.70 % ($D_{50} = 46$ nm) to 5 and 1 % at SS of 0.50 % ($D_{50} = 56$ nm) and 0.35 % ($D_{50} = 67$ nm), respectively. The fraction of non/less-hygroscopic hydrocarbon-like organic aerosol (HOA) decreased with increasing particle size (Lee et al., 2013). It contributes little to N_{CCN} by itself but the assumption of internal mixing allows it to contribute to CCN due to its mixing with more hygroscopic species and leads to an overestimated N_{CCN} (Rose et al., 2011; Wang et al., 2010). Size-resolved EC was not available and EC might also have caused the overestimation in N_{CCN} prediction. When SS decreased, D_{50} increased and the impact of HOAs on the N_{CCN} predictions decreased because of its smaller abundance relative to the hygroscopic inorganics. The large deviation in N_{CCN} prediction at $\text{SS} = 0.15$ % may be due to the uncertainty in the low number counts of CCN measurements or the high sensitivity of N_{CCN} to hygroscopicity at low SS as discussed later.

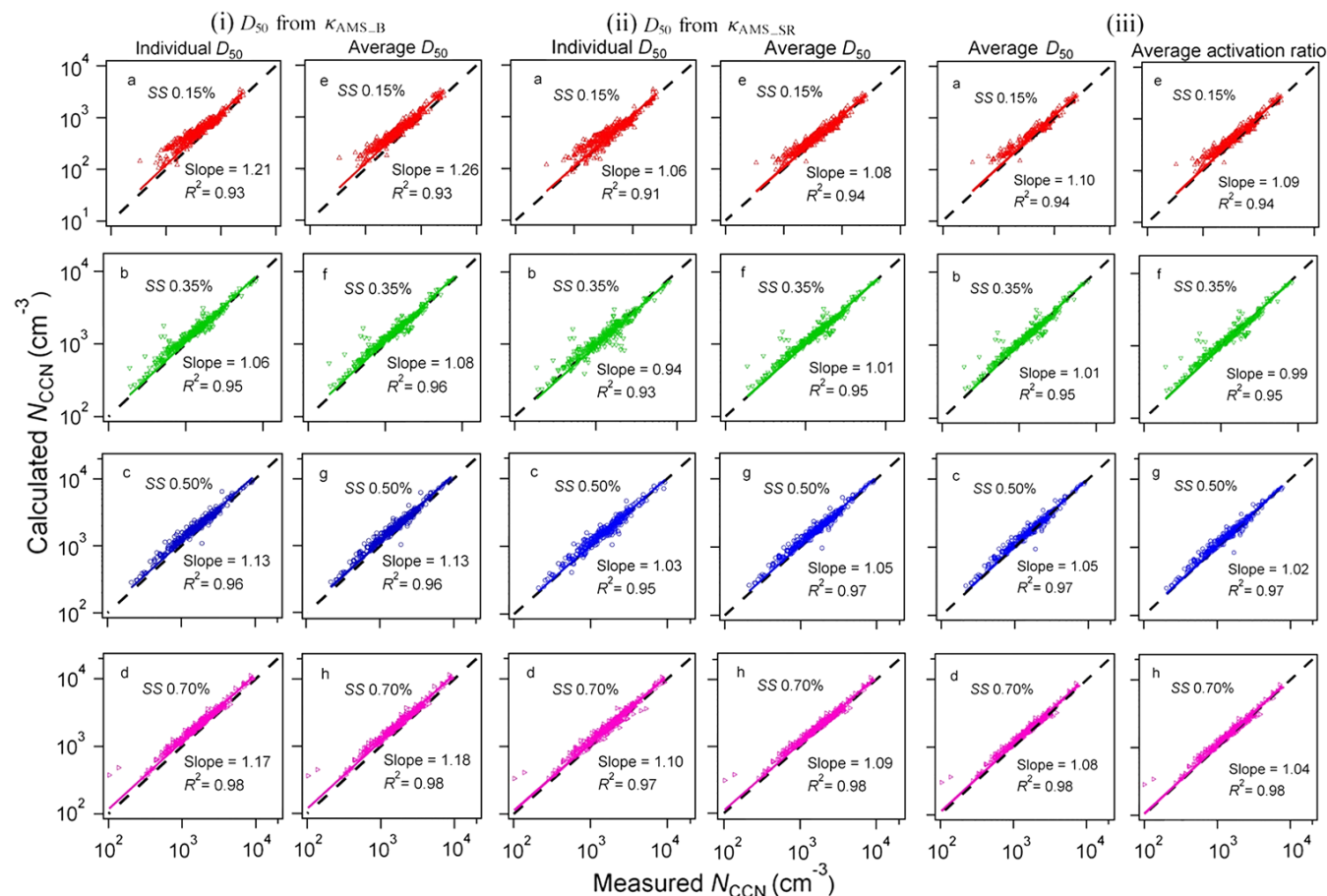


Figure 5. Calculations of N_{CCN} based on (i) (a–d) the individual D_{50} and (e–h) the average D_{50} over the whole period from κ_{AMS_B} , (ii) (a–d) the individual D_{50} and (e–h) the average D_{50} over the whole period from κ_{AMS_SR} and (iii) (a–d) the average D_{50} and (e–h) the average size-resolved CCN activation ratio from CCN measurement over the whole period.

3.3.2 Prediction of N_{CCN} from the constant κ

A constant $\kappa = 0.30$ has been proposed for predicting N_{CCN} and understanding the indirect effects of continental aerosols on climate on a global modeling scale (Andreae and Rosenfeld, 2008; Pringle et al., 2010). Rose et al. (2011) showed that the deviations between the measured and predicted N_{CCN} were less than 20% when they used an averaged $\kappa = 0.30$ over the course of their campaign in PRD in 2006. We evaluated the use of constant $\kappa = 0.30$, 0.33 (the average κ_{AMS_SR} over the campaign at the four SS), and 0.35 to estimate N_{CCN} . Overall, using $\kappa = 0.35$ overestimated N_{CCN} at all four SS while using 0.33 and 0.30 underestimated it at low SS $\leq 0.35\%$ and overestimated it at high SS $\geq 0.50\%$, respectively, as shown in Fig. S4 in the Supplement and Table 4. The slopes for $\kappa = 0.30$, 0.33 and 0.35 are quite different (0.91, 0.98 and 1.05) at SS = 0.15%, while they are much closer (1.11, 1.12 and 1.13) at SS = 0.70%. The difference in N_{CCN} prediction for the three κ decreased gradually from 14% at SS = 0.15% to 2% at SS = 0.70%. These results further confirm that the prediction of N_{CCN} is less sensitive to

κ at high SS than at low one, and that the impact of hygroscopicity on the N_{CCN} prediction decreases with increasing SS.

The difference in the sensitivity of predicted N_{CCN} to hygroscopicity at different SS can also be attributed to the aerosol size distributions (Dusek et al., 2006; Ervens et al., 2007). The average aerosol size distribution over the whole period had a main mode at ~ 70 nm and a shoulder at ~ 30 nm (Fig. 6a) in this campaign. At SS = 0.15%, D_{50} is approximately 116 nm and on the right of the main mode (Fig. 6b), a slight variation of κ and D_{50} will cause a large change in N_{CCN} prediction. On the contrary, at SS = 0.70%, the corresponding $D_{50} = 46$ nm is on the left of the main mode (Fig. 6c), a variation of κ and D_{50} will have less impact on N_{CCN} prediction as the N_{CCN} is dominated by the mode at 70 nm.

In addition, we carried out the N_{CCN} prediction during the hazy period, when HOAs contribute to $\sim 25\%$ of organic aerosols (OAs) (Li et al., 2013), based on the average size-resolved (1) $\kappa_{AMS} = 0.33$ over the whole campaign period

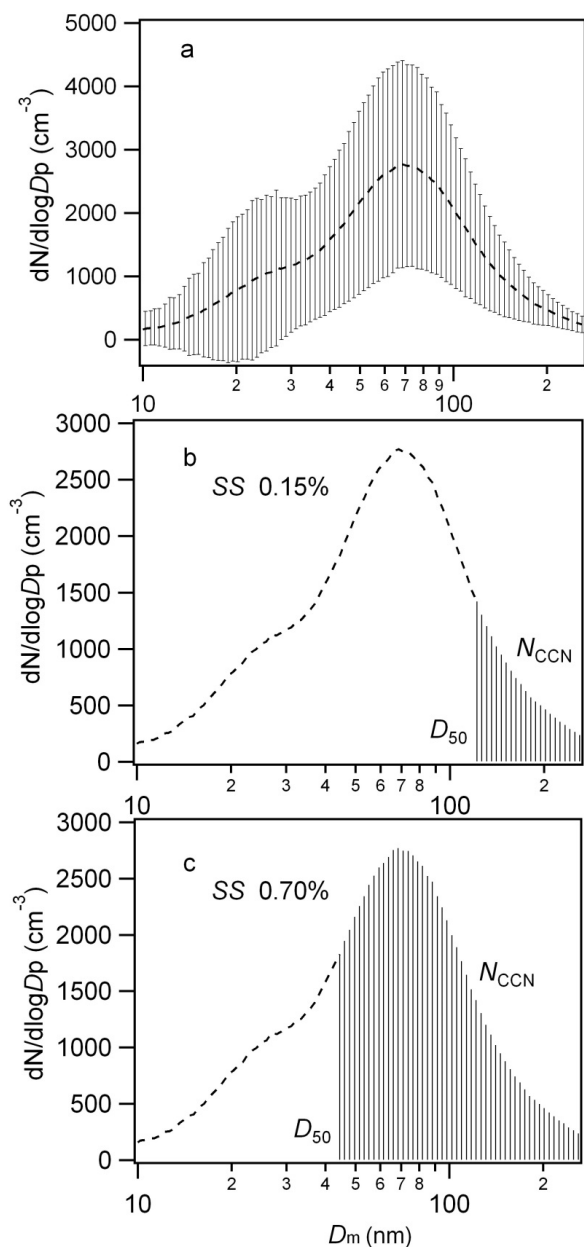


Figure 6. The average aerosol size distribution over the whole period (a), N_{CCN} prediction based on D_{50} at SS of 0.15 % (b) and 0.70 % (c). Data points are mean values and standard deviation.

and (2) $\kappa_{AMS} = 0.35$ over the hazy period only. As shown in Fig. S5 in the Supplement, using $\kappa_{AMS} = 0.33$ and 0.35 gave similar results with overestimations of 14 and 13 % at SS = 0.70 % respectively. In the hazy period, the assumption of internal mixing state allowed HOA-containing particles to act as CCN, thereby resulting in an overestimation of N_{CCN} by up to 14 %. At SS = 0.15 %, using $\kappa = 0.33$ led to an overestimation of just 2 %, while an overestimation of 9 % was found when using $\kappa = 0.35$. Overall, using $\kappa = 0.33$ gave pre-

dictions of N_{CCN} (Table 4) comparable to those using the κ_{AMS_SR} and better than those using κ_{AMS_B} at all four SS.

3.3.3 Mixing state and hygroscopicity

As discussed earlier, closure analysis based on hygroscopicity or D_{50} derived from chemical compositions assuming internal mixing alone cannot account for variability in the mixing state of aerosols, which could cause significant differences between predicted and measured N_{CCN} . In this section, we first calculate N_{CCN} by integrating the measured size-resolved N_{CN} distributions above the average D_{50} , obtained from the average CCN size-resolved activation ratio over the whole campaign. The second method involves integrating the product of the measured size distribution of N_{CN} and the average size-resolved N_{CCN} / N_{CN} activation ratio in each particle size bin. The size-resolved N_{CCN} / N_{CN} activation ratios reflect the influences of both the size-resolved chemical compositions and mixing state on CCN activity, and thus be used to examine the relative importance of mixing state and hygroscopicity in closure analysis compared to predictions assuming internal mixing state (Deng et al., 2013). The first method involves the hygroscopicity of aerosols as reflected by the value of D_{50} and the assumption of internal mixing while the second method involves hygroscopicity with actual mixing state information imbedded in the measured activation ratio curves. A comparison of the predictions of these two methods would give hints to the role of assumption of mixing states. Since D_{50} was obtained from the sigmoidal fits, those fits instead of actual data points were also used in the second method for better comparison. The average size-resolved CCN activation ratios at the four SS over the whole campaign are shown in Fig. S6 in the Supplement. Data points are shown as means \pm standard deviations.

The correlations of measured and predicted N_{CCN} based on the average D_{50} (a–d) and the average size-resolved activation ratio (e–h) are shown in Fig. 5(iii) a–d and e–h. The slopes of the fitted lines and R^2 at different SS are given in Table 4. The predicted and the measured N_{CCN} differed by less than 10 % using the average D_{50} . The difference is comparable to those using the average D_{50} from κ_{AMS_SR} (Fig. 5(ii) e–h). At SS = 0.70 %, using the average size-resolved CCN activation ratios reduced the overestimation from 8 % when using the average D_{50} to 4 %. As discussed above, the sensitivity of the N_{CCN} prediction to hygroscopicity is low at SS = 0.70 %, where a large change of 25 % in hygroscopicity from 0.28 to 0.35 result in only a variation within 5 % in N_{CCN} (Table 4). From the AMS measurements, the portion of non/less-hygroscopic species inferred by the fractions of f_{43} and f_{57} increased as the particle size decreased (Lee et al., 2013). Because of their higher abundance, their mixing with the hygroscopic components has a higher impact at SS = 0.70 % ($D_{50} = 46$ nm) than that at low SS = 0.15 % ($D_{50} = 116$ nm), where the reduction in the overestimation is minimal, from 10 % when using the

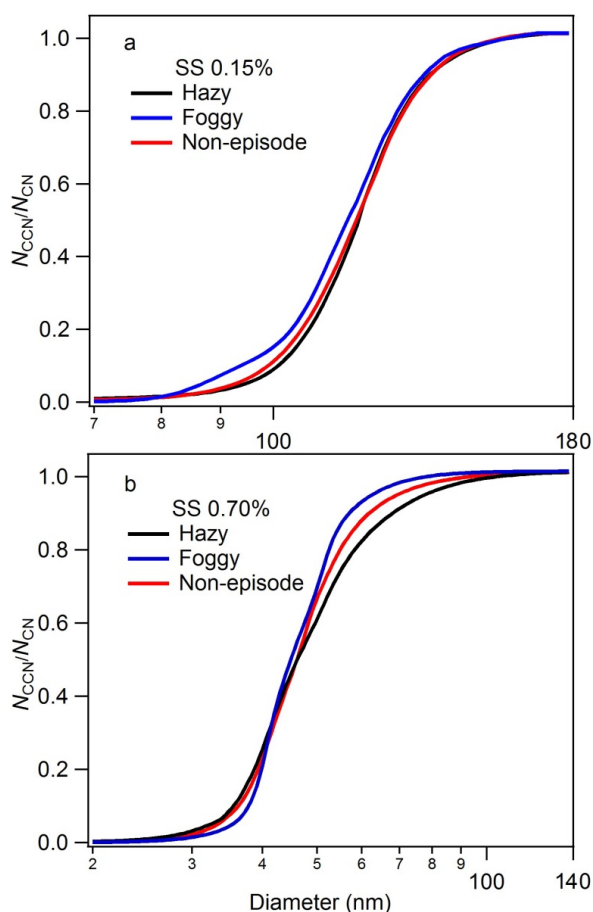


Figure 7. The average size-resolved CCN activation ratio at SS of (a) 0.15% and (b) 0.70% during the hazy, foggy and non-episode periods.

average D_{50} to 9% when using the average activation ratios approach. On the contrary, a difference of 19% was found when hygroscopicity increased from 0.30 to 0.39 at this low SS.

The average size-resolved activation ratios during the hazy, foggy and non-episode periods at SS = 0.15 and 0.7% are shown in Fig. 7. At SS = 0.15%, the activation ratios during the hazy and non-episode periods are similar but it is higher during the foggy period due possibly to the higher volume fraction of inorganics (Fig. 3d–f) and the smaller amount of non/less hygroscopic organics (Li et al., 2013). At SS = 0.70%, the CCN activation ratios of particles ranging from 50 to 100 nm in size are lower in the hazy period than in the non-episode period. The difference in the trends at SS = 0.15 and 0.70% may be due to the larger fractions of non/less hygroscopic species in smaller particles in the hazy period. These particles, which constitute a larger fraction of OAs in the hazy period than in the other periods, likely formed external mixtures with particles containing the aged particles of sulfate and the more oxidized (and hygroscopic) organics. Hence, a larger difference in the activation ratios

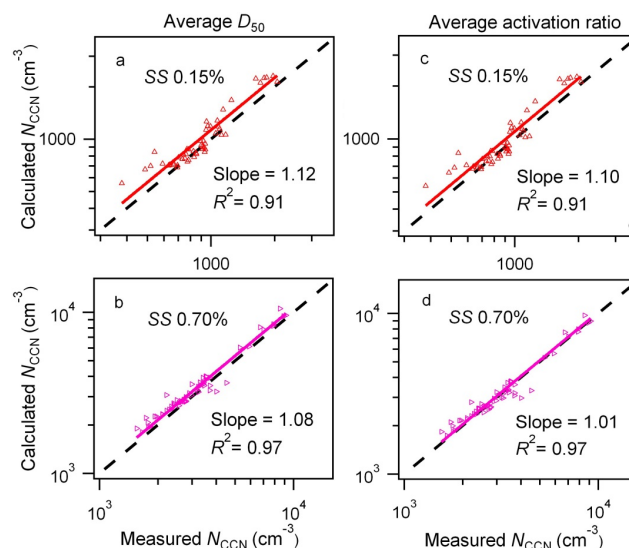


Figure 8. N_{CCN} estimation in hazy period based on (a and b) the average D_{50} and (c and d) the average size-resolved CCN activation ratio from CCN measurement over the hazy period.

between the hazy and the other periods could be observed at SS = 0.70% than at SS = 0.15%.

Figure 8 shows the N_{CCN} predicted based on the average D_{50} and the average size-resolved CCN activation ratio over the hazy period. At SS = 0.15%, using the average CCN activation ratio reduces overestimation from 12% when using average D_{50} to 10%. However, a much larger reduction from 8 to 1% was found at SS = 0.70%. This comparison supports that N_{CCN} prediction is likely more sensitive to mixing state than to hygroscopicity at high SS and vice versa at low SS.

4 Conclusion

In this study, a DMT CCNc-200 for N_{CCN} measurement, a TSI SMPS for N_{CN} measurement, and an Aerodyne HR-ToF-AMS for size-resolved and bulk PM_{10} chemical composition measurement were used to investigate the size-resolved CCN activity at a coastal site in Hong Kong in May 2011. Closure studies were carried out based on the κ_{AMS} estimated from bulk and size-resolved AMS measurement assuming internal mixing state. The deviation of N_{CCN} predicted from the individual D_{50} obtained from κ_{AMS} was similar to that predicted from the average D_{50} over the whole period at the four SS, which indicates that the average D_{50} well represented the aerosol CCN activation properties in this study. Using κ_{AMS_B} grossly over-predicted N_{CCN} by up to 26% because of the positive bias toward the inorganic fraction. On the contrary, the N_{CCN} predictions based on κ_{AMS_SR} were within 10% of the measurements. An accurate description of κ incorporating size-dependent compositions is necessary for good N_{CCN} predictions.

We compared the sensitivity of the N_{CCN} prediction to hygroscopicity (based on assumed internal mixing and κ estimates) and mixing state at different SS. N_{CCN} appears to be more sensitive to hygroscopicity than to mixing state at SS = 0.15 %, but the reverse is true at SS = 0.70 %. At SS = 0.15 %, D_{50} (116 nm) is larger than the mode diameter of the typical aerosol distributions we observed. A slight variation in κ (and D_{50}) would have a larger effect on N_{CCN} prediction than would at high SS = 0.70 %, where D_{50} (46 nm) is smaller than the mode diameter. The effect of mixing state is larger at SS = 0.70 %, which is associated with smaller particles having a higher percentage of non/less-hygroscopic components, than at SS = 0.15 %. Hygroscopicity is relatively less important to N_{CCN} prediction at this high SS.

The Supplement related to this article is available online at doi:10.5194/acp-14-10267-2014-supplement.

Acknowledgements. This work was supported by the University Grants Committee (Special Equipment Grant, SEG-HKUST07), Research Grants Council (GRF 600413) and the Environmental Conservation Funds (ECF) of Hong Kong (project number: ECWW09EG04).

Edited by: H. Su

References

- Alfarra, M. R., Paulsen, D., Gysel, M., Garforth, A. A., Dommen, J., Prévôt, A. S., Worsnop, D. R., Baltensperger, U., and Coe, H.: A mass spectrometric study of secondary organic aerosols formed from the photooxidation of anthropogenic and biogenic precursors in a reaction chamber, *Atmos. Chem. Phys.*, 6, 5279–5293, doi:10.5194/acp-6-5279-2006, 2006.
- Andreae, M. O. and Rosenfeld, D.: Aerosol-cloud-precipitation interactions. Part 1. The nature and sources of cloud-active aerosols, *Earth-Sci. Rev.*, 89, 13–41, 2008.
- Asa-Awuku, A., Nenes, A., Gao, S., Flagan, R. C., and Seinfeld, J. H.: Water-soluble SOA from Alkene ozonolysis: composition and droplet activation kinetics inferences from analysis of CCN activity, *Atmos. Chem. Phys.*, 10, 1585–1597, doi:10.5194/acp-10-1585-2010, 2010.
- Asa-Awuku, A., Moore, R. H., Nenes, A., Bahreini, R., Holloway, J. S., Brock, C. A., Middlebrook, A. M., Ryerson, T. B., Jimenez, J. L., and DeCarlo, P. F.: Airborne cloud condensation nuclei measurements during the 2006 Texas Air Quality Study, *J. Geophys. Res.-Atmos.*, 116, D11201, doi:10.1029/2010jd014874, 2011.
- Bougiatioti, A., Fountoukis, C., Kalivitis, N., Pandis, S., Nenes, A., and Mihalopoulos, N.: Cloud condensation nuclei measurements in the marine boundary layer of the Eastern Mediterranean: CCN closure and droplet growth kinetics, *Atmos. Chem. Phys.*, 9, 7053–7066, doi:10.5194/acp-9-7053-2009, 2009.
- Chan, C. K. and Yao, X.: Air pollution in mega cities in China, *Atmos. Environ.*, 42, 1–42, 2008.
- Chang, R. Y.-W., Slowik, J. G., Shantz, N. C., Vlasenko, A., Liggio, J., Sjostedt, S. J., Leaitch, W. R., and Abbatt, J. P. D.: The hygroscopicity parameter (κ) of ambient organic aerosol at a field site subject to biogenic and anthropogenic influences: relationship to degree of aerosol oxidation, *Atmos. Chem. Phys.*, 10, 5047–5064, doi:10.5194/acp-10-5047-2010, 2010.
- Cheng, Y. F., Eichler, H., Wiedensohler, A., Heintzenberg, J., Zhang, Y. H., Hu, M., Herrmann, H., Zeng, L. M., Liu, S., and Gnauk, T.: Mixing state of elemental carbon and non-light-absorbing aerosol components derived from in situ particle optical properties at Xinken in Pearl River Delta of China, *J. Geophys. Res.-Atmos.*, 111, D20204, doi:10.1029/2005jd006929, 2006.
- Cross, E. S., Slowik, J. G., Davidovits, P., Allan, J. D., Worsnop, D. R., Jayne, J. T., Lewis, D. K., Canagaratna, M., and Onasch, T. B.: Laboratory and ambient particle density determinations using light scattering in conjunction with aerosol mass spectrometry, *Aerosol Sci. Tech.*, 41, 343–359, 2007.
- Cubison, M. J., Ervens, B., Feingold, G., Docherty, K. S., Ulbrich, I. M., Shields, L., Prather, K., Hering, S., and Jimenez, J. L.: The influence of chemical composition and mixing state of Los Angeles urban aerosol on CCN number and cloud properties, *Atmos. Chem. Phys.*, 8, 5649–5667, doi:10.5194/acp-8-5649-2008, 2008.
- DeCarlo, P. F., Slowik, J. G., Worsnop, D. R., Davidovits, P., and Jimenez, J. L.: Particle morphology and density characterization by combined mobility and aerodynamic diameter measurements. Part I: Theory, *Aerosol Sci. Tech.*, 38, 1185–1205, 2004.
- DeCarlo, P. F., Kimmel, J. R., Trimborn, A., Northway, M. J., Jayne, J. T., Aiken, A. C., Gonin, M., Fuhrer, K., Horvath, T., Docherty, K. S., Worsnop, D. R., and Jimenez, J. L.: Field-deployable, high-resolution, time-of-flight aerosol mass spectrometer, *Anal. Chem.*, 78, 8281–8289, 2006.
- Deng, Z. Z., Zhao, C. S., Ma, N., Liu, P. F., Ran, L., Xu, W., Y. Chen, J., Liang, Z., Liang, S., Huang, M. Y., Ma, X. C., Zhang, Q., Quan, J. N., Yan, P., Henning, S., Mildenberger, K., Sommerhage, E., Schäfer, M., Stratmann, F., and Wiedensohler, A.: Size-resolved and bulk activation properties of aerosols in the North China Plain, *Atmos. Chem. Phys.*, 11, 3835–3846, doi:10.5194/acp-11-3835-2011, 2011.
- Deng, Z. Z., Zhao, C. S., Ma, N., Ran, L., Zhou, G. Q., Lu, D. R., and Zhou, X. J.: An examination of parameterizations for the CCN number concentration based on in situ measurements of aerosol activation properties in the North China Plain, *Atmos. Chem. Phys.*, 13, 6227–6237, doi:10.5194/acp-13-6227-2013, 2013.
- Dusek, U., Frank, G. P., Hildebrandt, L., Curtius, J., Schneider, J., Walter, S., Chand, D., Drewnick, F., Hings, S., Jung, D., Borrmann, S., and Andreae, M. O.: Size matters more than chemistry for cloud-nucleating ability of aerosol particles, *Science*, 312, 1375–1378, 2006.
- Ervens, B., Cubison, M., Andrews, E., Feingold, G., Ogren, J., Jimenez, J., Quinn, P., Bates, T., Wang, J., and Zhang, Q.: CCN predictions using simplified assumptions of organic aerosol composition and mixing state: a synthesis from six different locations, *Atmos. Chem. Phys.*, 10, 4795–4807, doi:10.5194/acp-10-4795-2010, 2010.
- Ervens, B., Cubison, M. J., Andrews, E., Feingold, G., Ogren, J. A., Jimenez, J. L., Quinn, P. K., Bates, T. S., Wang, J., Zhang, Q.,

- Coe, H., Flynn, M., and Allan, J. D.: Prediction of cloud condensation nucleus number concentration using measurements of aerosol size distributions and composition and light scattering enhancement due to humidity, *J. Geophys. Res.*, 112, D10S32, doi:10.1029/2006JD007426, 2007.
- Gong, Z., Lan, Z., Xue, L., Zeng, L., He, L., and Huang, X.: Characterization of submicron aerosols in the urban outflow of the central Pearl River Delta region of China, *Front. Environ. Sci. Eng.*, 6, 725–733, 2012.
- Gunthe, S. S., King, S. M., Rose, D., Chen, Q., Roldin, P., Farmer, D. K., Jimenez, J. L., Artaxo, P., Andreae, M. O., Martin, S. T., and Pöschl, U.: Cloud condensation nuclei in pristine tropical rainforest air of Amazonia: size-resolved measurements and modeling of atmospheric aerosol composition and CCN activity, *Atmos. Chem. Phys.*, 9, 7551–7575, doi:10.5194/acp-9-7551-2009, 2009.
- Gunthe, S. S., Rose, D., Su, H., Garland, R. M., Achtert, P., Nowak, A., Wiedensohler, A., Kuwata, M., Takegawa, N., Kondo, Y., Hu, M., Shao, M., Zhu, T., Andreae, M. O., and Pöschl, U.: Cloud condensation nuclei (CCN) from fresh and aged air pollution in the megacity region of Beijing, *Atmos. Chem. Phys.*, 11, 11023–11039, doi:10.5194/acp-11-11023-2011, 2011.
- Hersey, S. P., Craven, J. S., Schilling, K. A., Metcalf, A. R., Sorooshian, A., Chan, M. N., Flagan, R. C., and Seinfeld, J. H.: The Pasadena Aerosol Characterization Observatory (PACO): chemical and physical analysis of the Western Los Angeles basin aerosol, *Atmos. Chem. Phys.*, 11, 7417–7443, doi:10.5194/acp-11-7417-2011, 2011.
- Huang, X. H., Bian, Q., Ng, W. M., Louie, P. K., and Yu, J. Z.: Characterization of PM_{2.5} Major Components and Source Investigation in Suburban Hong Kong: A One Year Monitoring Study, *Aerosol Air Qual. Res.*, 14, 237–250, 2014.
- Kammermann, L., Gysel, M., Weingartner, E., Herich, H., Cziczó, D. J., Holst, T., Svenningsson, B., Arneth, A., and Baltensperger, U.: Subarctic atmospheric aerosol composition: 3. Measured and modeled properties of cloud condensation nuclei, *J. Geophys. Res.*, 115, D04202, doi:10.1029/2009JD012447, 2010.
- Kerminen, V.-M., Paramonov, M., Anttila, T., Riipinen, I., Fountoukis, C., Korhonen, H., Asmi, E., Laakso, L., Lihavainen, H., and Swietlicki, E.: Cloud condensation nuclei production associated with atmospheric nucleation: a synthesis based on existing literature and new results, *Atmos. Chem. Phys.*, 12, 12037–12059, doi:10.5194/acp-12-12037-2012, 2012.
- Kim, J. H., Yum, S. S., Shim, S., Yoon, S.-C., Hudson, J. G., Park, J., and Lee, S.-J.: On aerosol hygroscopicity, cloud condensation nuclei (CCN) spectra and critical supersaturation measured at two remote islands of Korea between 2006 and 2009, *Atmos. Chem. Phys.*, 11, 12627–12645, doi:10.5194/acp-11-12627-2011, 2011.
- King, S. M., Rosenoern, T., Shilling, J. E., Chen, Q., and Martin, S. T.: Cloud condensation nucleus activity of secondary organic aerosol particles mixed with sulfate, *Geophys. Res. Lett.*, 34, L24806, doi:10.1029/2007GL030390, 2007.
- Lambe, A. T., Onasch, T. B., Massoli, P., Croasdale, D. R., Wright, J. P., Ahern, A. T., Williams, L. R., Worsnop, D. R., Brune, W. H., and Davidovits, P.: Laboratory studies of the chemical composition and cloud condensation nuclei (CCN) activity of secondary organic aerosol (SOA) and oxidized primary organic aerosol (OPOA), *Atmos. Chem. Phys.*, 11, 8913–8928, doi:10.5194/acp-11-8913-2011, 2011.
- Lance, S., Nenes, A., Mazzoleni, C., Dubey, M. K., Gates, H., Varutbangkul, V., Rissman, T. A., Murphy, S. M., Sorooshian, A., and Flagan, R. C.: Cloud condensation nuclei activity, closure, and droplet growth kinetics of Houston aerosol during the Gulf of Mexico Atmospheric Composition and Climate Study (GoMACCS), *J. Geophys. Res.*, 114, D00F15, doi:10.1029/2008JD011699, 2009.
- Lance, S., Nenes, A., Medina, J., and Smith, J. N.: Mapping the operation of the DMT continuous flow CCN counter, *Aerosol Sci. Tech.*, 40, 242–254, 2006.
- Latham, T. L., Beyersdorf, A. J., Thornhill, K. L., Winstead, E. L., Cubison, M. J., Hecobian, A., Jimenez, J. L., Weber, R. J., Anderson, B. E., and Nenes, A.: Analysis of CCN activity of Arctic aerosol and Canadian biomass burning during summer 2008, *Atmos. Chem. Phys.*, 13, 2735–2756, doi:10.5194/acp-13-2735-2013, 2013.
- Latham, T. L. and Nenes, A.: Water vapor depletion in the DMT continuous-flow CCN chamber: Effects on supersaturation and droplet growth, *Aerosol Sci. Tech.*, 45, 604–615, 2011.
- Lee, B. P., Li, Y. J., Yu, J. Z., Louie, P. K., and Chan, C. K.: Physical and chemical characterization of ambient aerosol by HR-ToF-AMS at a suburban site in Hong Kong during springtime 2011, *J. Geophys. Res.-Atmos.*, 118, 8625–8639, doi:10.1002/jgrd.50658, 2013.
- Li, Y. J., Lee, B. Y. L., Yu, J. Z., Ng, N. L., and Chan, C. K.: Evaluating the degree of oxygenation of organic aerosol during foggy and hazy days in Hong Kong using high-resolution time-of-flight aerosol mass spectrometry (HR-ToF-AMS), *Atmos. Chem. Phys.*, 13, 8739–8753, doi:10.5194/acp-13-8739-2013, 2013.
- Li, Y. J., Lee, B. P., Su, L., Fung, J. C. H., and Chan, C. K.: Seasonal characteristics of fine particulate matter (PM) based on high resolution time-of-flight aerosol mass spectrometric (HR-ToF-AMS) measurements at the HKUST Supersite in Hong Kong, *Atmos. Chem. Phys. Discuss.*, 14, 20259–20293, doi:10.5194/acpd-14-20259-2014, 2014.
- Lopez-Yglesias, X. F., Yeung, M. C., Dey, S. E., Brechtel, F. J., and Chan, C. K.: Performance evaluation of the Brechtel Mfg. Humidified Tandem Differential Mobility Analyzer (BMI HTDMA) for studying hygroscopic properties of aerosol particles, *Aerosol Sci. Tech.*, 48, 969–980, doi:10.1080/02786826.2014.952366, 2014.
- Low, R. D. H.: A generalized equation for the solution effect in droplet growth, *J. Atmos. Sci.*, 26, 608–611, 1969.
- Massoli, P., Lambe, A. T., Ahern, A. T., Williams, L. R., Ehn, M., Mikkila, J., Canagaratna, M. R., Brune, W. H., Onasch, T. B., Jayne, J. T., Petaja, T., Kulmala, M., Laaksonen, A., Kolb, C. E., Davidovits, P., and Worsnop, D. R.: Relationship between aerosol oxidation level and hygroscopic properties of laboratory generated secondary organic aerosol (SOA) particles, *Geophys. Res. Lett.*, 37, L24801, doi:10.1029/2010GL045258, 2010.
- Medina, J., Nenes, A., Sotiropoulou, R. E. P., Cottrell, L. D., Ziemba, L. D., Beckman, P. J., and Griffin, R. J.: Cloud condensation nuclei closure during the International Consortium for Atmospheric Research on Transport and Transformation 2004 campaign: Effects of size-resolved composition, *J. Geophys. Res.*, 112, D10S31, doi:10.1029/2006JD007588, 2007.

- Mei, F., Setyan, A., Zhang, Q., and Wang, J.: CCN activity of organic aerosols observed downwind of urban emissions during CARES, *Atmos. Chem. Phys.*, 13, 12155–12169, doi:10.5194/acp-13-12155-2013, 2013.
- Moore, R. H., Cerully, K., Bahreini, R., Brock, C. A., Middlebrook, A. M., and Nenes, A.: Hygroscopicity and composition of California CCN during summer 2010, *J. Geophys. Res.-Atmos.*, 117, D00V12, doi:10.1029/2011JD017352, 2012a.
- Moore, R. H., Nenes, A., and Medina, J.: Scanning mobility CCN analysis-A method for fast measurements of size-resolved CCN distributions and activation kinetics, *Aerosol Sci. Tech.*, 44, 861–871, 2010.
- Moore, R. H., Raatikainen, T., Langridge, J. M., Bahreini, R., Brock, C. A., Holloway, J. S., Lack, D. A., Middlebrook, A. M., Perring, A. E., Schwarz, J. P., Spackman, J. R., and Nenes, A.: CCN spectra, hygroscopicity, and droplet activation kinetics of secondary organic aerosol resulting from the 2010 Deepwater Horizon oil spill, *Environ. Sci. Tech.*, 46, 3093–3100, 2012b.
- Padró, L. T., Moore, R. H., Zhang, X., Rastogi, N., Weber, R. J., and Nenes, A.: Mixing state and compositional effects on CCN activity and droplet growth kinetics of size-resolved CCN in an urban environment, *Atmos. Chem. Phys.*, 12, 10239–10255, doi:10.5194/acp-12-10239-2012, 2012.
- Padró, L. T., Tkacik, D., Latham, T., Hennigan, C. J., Sullivan, A. P., Weber, R. J., Huey, L. G., and Nenes, A.: Investigation of cloud condensation nuclei properties and droplet growth kinetics of the water soluble aerosol fraction in Mexico City, *J. Geophys. Res.-Atmos.*, 115, D09204, doi:10.1029/2009jd013195, 2010.
- Petters, M. D. and Kreidenweis, S. M.: A single parameter representation of hygroscopic growth and cloud condensation nucleus activity, *Atmos. Chem. Phys.*, 7, 1961–1971, doi:10.5194/acp-7-1961-2007, 2007.
- Petters, M. D. and Kreidenweis, S. M.: A single parameter representation of hygroscopic growth and cloud condensation nucleus activity – Part 3: Including surfactant partitioning, *Atmos. Chem. Phys.*, 13, 1081–1091, doi:10.5194/acp-13-1081-2013, 2013.
- Pringle, K. J., Tost, H., Pozzer, A., Pöschl, U., and Lelieveld, J.: Global distribution of the effective aerosol hygroscopicity parameter for CCN activation, *Atmos. Chem. Phys.*, 10, 5241–5255, doi:10.5194/acp-10-5241-2010, 2010.
- Roberts, G. C. and Nenes, A.: A continuous-flow streamwise thermal-gradient CCN chamber for atmospheric measurements, *Aerosol Sci. Tech.*, 39, 206–221, 2005.
- Rose, D., Gunthe, S. S., Mikhailov, E., Frank, G. P., Dusek, U., Andreae, M. O., and Pöschl, U.: Calibration and measurement uncertainties of a continuous-flow cloud condensation nuclei counter (DMT-CCNC): CCN activation of ammonium sulfate and sodium chloride aerosol particles in theory and experiment, *Atmos. Chem. Phys.*, 8, 1153–1179, doi:10.5194/acp-8-1153-2008, 2008.
- Rose, D., Nowak, A., Achtert, P., Wiedensohler, A., Hu, M., Shao, M., Zhang, Y., Andreae, M. O., and Pöschl, U.: Cloud condensation nuclei in polluted air and biomass burning smoke near the mega-city Guangzhou, China – Part 1: Size-resolved measurements and implications for the modeling of aerosol particle hygroscopicity and CCN activity, *Atmos. Chem. Phys.*, 10, 3365–3383, doi:10.5194/acp-10-3365-2010, 2010.
- Rose, D., Gunthe, S. S., Su, H., Garland, R. M., Yang, H., Berghof, M., Cheng, Y. F., Wehner, B., Achtert, P., Nowak, A., Wiedensohler, A., Takegawa, N., Kondo, Y., Hu, M., Zhang, Y., Andreae, M. O., and Pöschl, U.: Cloud condensation nuclei in polluted air and biomass burning smoke near the mega-city Guangzhou, China – Part 2: Size-resolved aerosol chemical composition, diurnal cycles, and externally mixed weakly CCN-active soot particles, *Atmos. Chem. Phys.*, 11, 2817–2836, doi:10.5194/acp-11-2817-2011, 2011.
- Stroud, C. A., Nenes, A., Jimenez, J. L., DeCarlo, P. F., Huffman, J. A., Bruinijtes, R., Nemitz, E., Delia, A. E., Toohey, D. W., Guenther, A. B., and Nandi, S.: Cloud activating properties of aerosol observed during CELTIC, *J. Atmos. Sci.*, 64, 441–459, 2007.
- Sueper, D.: ToF-AMS data analysis software: <http://cires.colorado.edu/jimenez-group/ToFAMSResources/ToFSoftware/index.html> (last access: 1 June 2012), 2011.
- Sullivan, R. C., Moore, M. J. K., Petters, M. D., Kreidenweis, S. M., Roberts, G. C., and Prather, K. A.: Effect of chemical mixing state on the hygroscopicity and cloud nucleation properties of calcium mineral dust particles, *Atmos. Chem. Phys.*, 9, 3303–3316, doi:10.5194/acp-9-3303-2009, 2009.
- Takegawa, N., Miyakawa, T., Watanabe, M., Kondo, Y., Miyazaki, Y., Han, S., Zhao, Y., Van Pinxteren, D., Brüggemann, E., Gnauk, T., Herrmann, H., Xiao, R., Deng, Z., Hu, M., Zhu, T., and Zhang, Y.: Performance of an Aerodyne aerosol mass spectrometer (AMS) during intensive campaigns in China in the summer of 2006, *Aerosol Sci. Tech.*, 43, 189–204, 2009.
- Tang, I. N. and Munkelwitz, H. R.: Water activities, densities, and refractive indices of aqueous sulfates and sodium nitrate droplets of atmospheric importance, *J. Geophys. Res.-Atmos.*, 99, 18801–18818, doi:10.1029/94jd01345, 1994.
- Textor, C., Schulz, M., Guibert, S., Kinne, S., Balkanski, Y., Bauer, S., Bernsten, T., Berglen, T., Boucher, O., Chin, M., Dentener, F., Diehl, T., Easter, R., Feichter, H., Fillmore, D., Ghan, S., Ginoux, P., Gong, S., Grini, A., Hendricks, J., Horowitz, L., Huang, P., Isaksen, I., Iversen, I., Kloster, S., Koch, D., Kirkevåg, A., Kristjansson, J. E., Krol, M., Lauer, A., Lamarque, J. F., Liu, X., Montanaro, V., Myhre, G., Penner, J., Pitari, G., Reddy, S., Seland, Ø., Stier, P., Takemura, T., and Tie, X.: Analysis and quantification of the diversities of aerosol life cycles within AeroCom, *Atmos. Chem. Phys.*, 6, 1777–1813, doi:10.5194/acp-6-1777-2006, 2006.
- Wang, J., Cubison, M. J., Aiken, A. C., Jimenez, J. L., and Collins, D. R.: The importance of aerosol mixing state and size-resolved composition on CCN concentration and the variation of the importance with atmospheric aging of aerosols, *Atmos. Chem. Phys.*, 10, 7267–7283, doi:10.5194/acp-10-7267-2010, 2010.
- Wang, S. C. and Flagan, R. C.: Scanning electrical mobility spectrometer, *Aerosol Sci. Tech.*, 13, 230–240, 1990.
- Wex, H., McFiggans, G., Henning, S., and Stratmann, F.: Influence of the external mixing state of atmospheric aerosol on derived CCN number concentrations, *Geophys. Res. Lett.*, 37, L10805, doi:10.1029/2010gl043337, 2010.
- Xiao, R., Takegawa, N., Zheng, M., Kondo, Y., Miyazaki, Y., Miyakawa, T., Hu, M., Shao, M., Zeng, L., Gong, Y., Lu, K., Deng, Z., Zhao, Y., and Zhang, Y. H.: Characterization and source apportionment of submicron aerosol with aerosol mass spectrometer during the PRIDE-PRD 2006 campaign, *Atmos. Chem. Phys.*, 11, 6911–6929, doi:10.5194/acp-11-6911-2011, 2011.

- Yeung, M. C., Lee, B. P., Li, Y. J., and Chan, C. K.: Simultaneous HTDMA and HR-ToF-AMS measurements at the HKUST Supersite in Hong Kong in 2011, *J. Geophys. Res.-Atmos.*, 119, 9864–9883, doi:10.1002/2013JD021146, 2014.
- Young, K. C. and Warren, A. J.: A reexamination of the derivation of the equilibrium supersaturation curve for soluble particles, *J. Atmos. Sci.*, 49, 1138–1143, 1992.
- Zhang, Z., Engling, G., Lin, C.-Y., Chou, C. C.-K., Lung, S.-C. C., Chang, S.-Y., Fan, S., Chan, C.-Y., and Zhang, Y.-H.: Chemical speciation, transport and contribution of biomass burning smoke to ambient aerosol in Guangzhou, a mega city of China, *Atmos. Environ.*, 44, 3187–3195, 2010.